High-harmonic generation from hydrogen atoms driven by two-color mutually orthogonal laser fields

Mitsuko Murakami*
Center for Quantum Science and Engineering, and Center for Advanced Study in Theoretical Sciences, Department of Physics, National Taiwan University, Taipei 10617, Taiwan

Oleg Korobkin
Oskar Klein Center, Department of Astronomy, Stockholm University, AlbaNova, SE-10691 Stockholm, Sweden

Marko Horbatsch
Department of Physics and Astronomy, York University, Toronto, Ontario, Canada M3J 1P3
(Received 20 June 2013; published 27 December 2013)

Calculations of high-harmonic spectra from hydrogen atoms driven by strong two-color orthogonal fields with wavelengths 800 and 400 nm are presented. The azimuthal symmetry of the electron dynamics is broken by the two-color orthogonal fields, and therefore the fully three-dimensional time-dependent Schrödinger equation is solved by using the generalized pseudospectral method. The cycle-averaged collision angles as a function of phase delay between the orthogonal fields are evaluated from the harmonic spectra. The results are in qualitative agreement with a recent experiment with helium atoms. Furthermore, the timing and direction of recollisions during the high-harmonic generation are analyzed in the time-frequency domain to extract electron trajectory information on subcycle time scales. Comparison with recent model calculations is also made.

DOI: 10.1103/PhysRevA.88.063419 PACS number(s): 32.80.Rm, 42.65.Ky

I. INTRODUCTION

In recent years, a new type of measurement has been introduced in the field of high-harmonic generation (HHG) with potential applications for laser tomography [1–4]. In these experiments, two mutually orthogonal laser fields of different frequencies (colors) and intensities are used to ionize atoms or molecules. An intense fundamental field is supplemented by a perpendicular and weaker secondary field with doubled frequency, so that the motion of the ionized electrons is preferentially along the direction of the fundamental field. Ionized electrons may recollide efficiently with parent ions to produce high-harmonic radiation [5].

The situation is different from when a circularly polarized laser field is applied, where electrons are driven at equal strength and frequency in the two orthogonal directions; in this case, they tend to permanently ionize rather than recollide. The circularly polarized driving laser is useful for the study of above-threshold ionization, as it eliminates the rescattered electrons that can contaminate the analysis of pure ionization [6–8]. For laser tomography applications, however, one relies on high-harmonic spectra for structural information of the source atoms or molecules, and therefore a linearly polarized field has traditionally been used to promote recollisions, in combination with the molecular alignment technique [9]. The HHG in two-color orthogonal fields is an alternative approach and useful particularly for the tomography of atoms because it is impossible to orient the atoms as is done for linear molecules. In order to record the multidimensional structure, electrons must recollide with parent ions at many different angles, not just along one direction as in the linearly polarized laser field. Two-color orthogonal fields induce the multidimensional recollisions that are necessary for the tomography measurement. In this context, the issue of tunneling time has also been addressed very recently [10,11].

In this paper, electron dynamics in two-color orthogonal fields are investigated using numerical solutions of the time-dependent Schrödinger equation (TDSE) for the hydrogen atom. In particular, we evaluate the angle of recollisions from hydrogen high-harmonic spectra on the basis of forming ratios of even- and odd-order harmonic yield, in analogy to the measurements in Ref. [1] with helium and neon atoms. We extend the generalized pseudospectral (GPS) method [12] to discretize the TDSE in three dimensions, since it is computationally less expensive and more accurate than finite difference methods. There are some published numerical studies of laser-atom interactions in three dimensions, dealing mainly with elliptically polarized fields [6,13,14], but only few with two-color orthogonal fields [15]. Our calculated recollision angles as a function of time delay between the two fields qualitatively agree with the experiment for helium atoms in Ref. [1].

One of our purposes is to complement the calculation based on the strong-field approximation (SFA) which accompanied the experiment in Ref. [3] and showed that the relative phase between the two orthogonal fields can be used to control the electron trajectories at the single-atom level. We analyze harmonic spectra in the time-frequency domain using the Gabor transform [16] to gain insight into the trajectory interference in two-color orthogonal fields. This time-frequency analysis also provides theoretical support for the time-resolved measurement of electron dynamics using the HHG driven by two-color orthogonal fields [10]. The time information extracted from the Gabor transforms of the hydrogen harmonic spectra shows features similar to those obtained by Zhao and Lein [11] for their model helium atom.

*mitsuko@phys.ntu.edu.tw

The paper is organized as follows. First, we describe our theoretical methods in Sec. II. In Sec. II A, the GPS calculation of the TDSE for the hydrogen atom is introduced. The three-dimensional (3D) time-evolution scheme and the evaluation of harmonic spectra for the two-color orthogonal fields are explained in Secs. II B and II C, respectively. The determination of collision angles according to a prescription given in Ref. [1] is summarized in Sec. II D, and Sec. II E introduces a method to calculate time-resolved collision angles using the Gabor transform of harmonic fields. Section III comprises our results. In Sec. III A, we examine ionization rates of the hydrogen atom in two-color orthogonal fields in comparison with linearly and circularly polarized laser fields for three different peak intensities. Sample harmonic spectra of the hydrogen atom driven by a 20-cycle, two-color (800 + 400 nm) orthogonal field of fundamental-field intensity 1×10^{14} W cm^{-2} are presented in Sec. III B, and the corresponding collision angles as a function of phase delay between the two orthogonal fields are shown in Sec. III C. The spectra in Sec. III B are studied further in the time-frequency domain using the Gabor transform in Sec. III D. Last, the time-resolved collision angles for selected phase delays are evaluated also by using the Gabor transform and discussed in Sec. III E. Section IV concludes the paper. Atomic units ($\hbar = m_e = e = 1$) are used throughout, unless specified otherwise.

II. THEORETICAL METHODS

A. Generalized pseudospectral method for the hydrogen atom

This section summarizes the GPS method for the hydrogen atom, originally developed in Ref. [12]. The wave function of the hydrogen atom is expanded using spherical harmonics $Y_\ell^m(\theta,\phi)$ as

$$\psi(\vec{r},t) = \sum_{\ell,m} \frac{R_\ell^m(r,t)}{r} Y_\ell^m(\theta,\phi), \tag{1}$$

where $\ell = 0,1,2,\ldots,N_\ell$ and $|m| \leqslant \ell$. The radial coordinate $r \in [0,r_{\max}]$ is mapped into the interval $x \in [-1,1]$ as

$$r(x) = L\frac{1+x}{1-x+\alpha} \quad \left(\alpha = \frac{2L}{r_{\max}}\right), \tag{2}$$

where L is an arbitrary constant. Then, the radial function $R_\ell^m(r,t)$ in Eq. (1) is interpolated at the Legendre-Lobatto collocation points:

$$\left\{x_j : \left(1-x_j{}^2\right) P_N{}'(x_j) = 0\right\} \quad (j = 0,1,2,\ldots N), \tag{3}$$

where $P_N{}'$ is the first derivative of the Nth-order Legendre polynomial P_N. Furthermore, we introduce the following discretized wave function:

$$\varphi_\ell^m(x_j,t) = R_\ell^m(r(x_j),t)\frac{\sqrt{r'(x_j)}}{P_N(x_j)}\sqrt{\frac{2}{N(N+1)}} \quad (j = 1,2,\ldots,N-1). \tag{4}$$

Its normalization condition (without the presence of absorbing boundaries) is simply

$$\sum_{\ell,m,j} \left|\varphi_\ell^m(x_j,t)\right|^2 = 1. \tag{5}$$

The stationary Hamiltonian for $\varphi_\ell^m(x_j)$ is given by

$$\mathcal{H}_0(\ell) = \frac{-1}{2}\frac{\partial^2}{\partial r^2} + \frac{\ell(\ell+1)}{2r^2(x_j)} - \frac{1}{r(x_j)}. \tag{6}$$

The symmetrized matrix form of $\mathcal{H}_0(\ell)$ is given in Ref. [12].

B. Atom-laser interaction in the two-color orthogonal fields

The electric-field vector for two-color orthogonal fields is given by

$$\vec{E}(t) = E_o(t)\left[\hat{\mathbf{z}}\cos(\omega_o t) + \hat{\mathbf{x}}\left(\tfrac{1}{2}\cos(2\omega_o t + \beta)\right)\right], \tag{7}$$

where $E_o(t)$ is an envelope function, and β is the phase delay between the fundamental and the secondary fields. For all calculations in this work, the envelope function is $E_o(t) = E_o\cos^2(\pi t/\tau)$ centered around $t = 0$ and has a duration of $\tau = 20$ optical cycles. The absorbing boundary is set to start at five times the classical electron oscillation radius $E_o/{\omega_o}^2$. The strength of the secondary field (along the x axis) is kept at a half of the fundamental field (along the z axis), to be consistent with the experiments in Refs. [1] and [3]. This leads to a 4:1 ratio for the driving-laser intensity between the two orthogonal directions. The corresponding time-dependent potential is therefore

$$V(\vec{r},t) = E_o(t)r\big[\cos\theta\cos(\omega_o t) + \tfrac{1}{2}\sin\theta\cos\phi\cos(2\omega_o t + \beta)\big]. \tag{8}$$

The ϕ dependence in $V(\vec{r},t)$ means that it mixes different m states, as well as ℓ states. Our strategy in this case is to apply the time-dependent evolution operator in the (θ,ϕ) space rather than the (ℓ,m) space using a split-operator technique:

$$\varphi_{\ell'}^{m'}(x_j{}',t+\Delta t) \simeq e^{-i\mathcal{H}_0(\ell)\Delta t/2}\mathcal{S}^{-1}(\ell',m')e^{-iV(\vec{r},t+\Delta/2)\Delta t} \times \mathcal{S}(\theta_\lambda,\phi_\mu)e^{-i\mathcal{H}_0(\ell)\Delta t/2}\varphi_\ell^m(x_j,t), \tag{9}$$

where $\mathcal{S}$ denotes the spherical harmonic transform [17], i.e.,

$$\mathcal{S}\left\{\varphi_\ell^m(x_j,t)\right\}(\theta_\lambda,\phi_\mu) = \frac{1}{\sqrt{2\pi}}\sum_{\ell,m} e^{im\phi_\mu}\sqrt{\frac{(2\ell+1)(\ell-m)!}{2(\ell+m)!}} \times P_\ell^m(\cos\theta_\lambda)\,\varphi_\ell^m(x_j,t) = \varphi(x_j,\theta_\lambda,\phi_\mu,t), \tag{10}$$

and provides the change in representation. Here $\{\phi_\mu\}$ is a set of uniform grid points along the azimuthal angles:

$$\phi_\mu = \frac{2\pi\mu}{2N_\ell+1} \quad (\mu = 0,1,2,\ldots,2N_\ell), \tag{11}$$

whereas a set of discretized polar angles $\{\theta_\lambda\}$, given by

$$\theta_\lambda = \frac{\pi\lambda}{N_\ell} \quad (\lambda = 0,1,2,\ldots,N_\ell), \tag{12}$$

is mapped using a transformation $y_\lambda = \cos\theta_\lambda$ onto the set of Legendre-Gauss collocation points:

$$\{y_\lambda : P_{N_\ell+1}(y_\lambda) = 0\}. \tag{13}$$

The inverse transform $\mathcal{S}^{-1}$ takes $\{\varphi(x_j,\theta_\lambda,\phi_\mu,t)\}$ back into the (ℓ,m) space.

For calculations using $800 + 400$ nm driving lasers, the number of points along the radial direction is chosen in the range $N = 250$–450, depending on the intensities considered (0.5–2×10^{14} W cm^{-2}), and the maximum angular momentum is set by $N_\ell = 63$. The time step is $\Delta t = 0.2$.

C. Evaluation of harmonic spectra

From Ehrenfest's theorem, the z component of the acceleration operator is given by [18]

$$a_z = -[\mathcal{H},[\mathcal{H},z]] = \left[\mathcal{H},\frac{\partial}{\partial r}\right]\cos\theta, \tag{14}$$

where $\mathcal{H}$ is the full Hamiltonian including the laser interaction. To obtain its expectation value $\langle a_z\rangle$ at each time step, we find expressions of the matrix elements $\langle \ell+1,m|a_z|\ell m\rangle$ in terms of the reduced matrix elements $\langle \ell+1||a_z||\ell\rangle$, as outlined in Ref. [19]. The result is

$$\langle a_z\rangle = \sum_{\ell,m,j} c_\ell^m \left(\frac{\ell^2}{r^3(x_j)} - \frac{1}{r^2(x_j)}\right)\mathbf{Re}\left[\varphi_{\ell+1}^{m\,*}(x_j)\varphi_\ell^m(x_j)\right], \tag{15}$$

where

$$c_\ell^m = \sqrt{\frac{(\ell+m+1)(\ell-m+1)}{(2\ell+1)(2\ell+3)}}. \tag{16}$$

The terms proportional to the fundamental field were dropped in Eq. (15) because they do not contribute to high-harmonic spectra. Similarly, the x component of the acceleration operator is

$$a_x = -[\mathcal{H},[\mathcal{H},x]] = \left[\mathcal{H},\frac{\partial}{\partial r}\right]\sin\theta\cos\phi. \tag{17}$$

Therefore, its expectation value is evaluated from the matrix elements $\langle \ell+1,m\pm1|a_x|\ell m\rangle$ as

$$\langle a_x\rangle = \sum_{\ell,m,j}\left(\frac{\ell^2}{r^3(x_j)} - \frac{1}{r^2(x_j)}\right)\frac{1}{2}\,\mathbf{Re}\left[\kappa_\ell^m \varphi_\ell^{m\,*}(x_j)\varphi_{\ell+1}^{m+1}(x_j) + \kappa_\ell^{-m}\varphi_\ell^{m\,*}(x_j)\varphi_{\ell+1}^{m-1}(x_j)\right], \tag{18}$$

where

$$\kappa_\ell^m = \sqrt{\frac{(\ell+m+1)(\ell+m+2)}{(2\ell+1)(2\ell+3)}}. \tag{19}$$

Once the time sequence of accelerations $\langle a_{z,x}\rangle(t,\beta)$ is obtained from solutions of the TDSE, the high-harmonic spectra are found as

$$D(\omega,\beta) = |\tilde{a}_z(\omega,\beta)|^2 + |\tilde{a}_x(\omega,\beta)|^2, \tag{20}$$

where the respective components of the acceleration expectation values are transformed using

$$\tilde{a}_{z,x}(\omega,\beta) = \frac{1}{t_f - t_i}\frac{1}{\omega^2}\int_{t_i}^{t_f} dt\; e^{-i\omega t}\langle a_{z,x}\rangle(t,\beta). \tag{21}$$

D. Recollision angles

It is known that a two-color, orthogonal driving laser produces both odd- and even-order high-harmonic fields [1–3]. The nth harmonic field can be expressed in terms of dipole transition matrix elements A_z and A_x along the two orthogonal axes as [20]

$$\vec{E}_n \propto A_z\hat{\mathbf{z}} + A_x\hat{\mathbf{x}} - e^{-in\pi}(A_z\hat{\mathbf{z}} - A_x\hat{\mathbf{x}}). \tag{22}$$

The first two terms in Eq. (22) are induced by the first half of each driving-laser cycle, and the last two terms by the second half cycle. The negative sign for A_x in the last term is due to the doubled frequency in the secondary field. It then follows that

$$\vec{E}_{\rm odd} \propto A_z\hat{\mathbf{z}}, \quad \vec{E}_{\rm even} \propto A_x\hat{\mathbf{x}}. \tag{23}$$

Thus, odd- and even-order harmonics generated by the two-color orthogonal driving fields are polarized exclusively along the fundamental and the secondary field vectors, respectively. Based on this fact, the recollision angles of ionized electrons with the parent ions (He^+ and Ne^+) can be inferred from harmonic spectra in Ref. [1] according to

$$|\theta_{\rm rec}(\omega,\beta)| = \arctan\left(\sqrt{\frac{I_{\rm even}(\omega,\beta)}{I_{\rm odd}(\omega,\beta)}}\right), \tag{24}$$

where $I_{\rm odd} = |\vec{E}_{\rm odd}|^2$ and $I_{\rm even} = |\vec{E}_{\rm even}|^2$. Note that the adjacent harmonics are interpolated to obtain continuous spectra separately for even- and odd-order harmonics before taking their intensity ratio. In Sec. III C, we present the recollision angles evaluated using Eq. (24) for hydrogen atoms.

E. Time-frequency representation of harmonic fields

In Sec. III D, we examine Gabor transforms of harmonic spectra to study the timing of the recollision process in HHG driven by the two-color orthogonal fields. The Gabor transform is a time-frequency representation of a harmonic field, defined by [16]

$$G_{z,x}(t,\omega,\beta) = \left|\int dt'\, e^{-i\omega t'}\,\langle a_{z,x}\rangle(t',\beta)\,E_G(t'-t)\right|^2, \tag{25}$$

where

$$E_G(t) = \frac{\exp\left[-t^2/2{\sigma_o}^2\right]}{\sqrt{2\pi}\sigma_o}. \tag{26}$$

The sweeping function $E_G(t)$ needs to be sufficiently short to resolve the subcycle structure in the harmonic field. We set the full width at half maximum in Eq. (25) to $\sigma_o = (3\omega_o)^{-1}$ for this purpose [16]. Moreover, in analogy to Eq. (24), we then calculate the *time-resolved* recollision angles as

$$|\theta_{\rm rec}(\omega,t,\beta)| = \arctan\left(\sqrt{\frac{G_x(\omega,t,\beta)}{G_z(\omega,t,\beta)}}\right). \tag{27}$$

In Sec. III E, the time-resolved recollision angles for fixed phase delays are investigated.

III. RESULTS

A. Ionization rates

The norm of the wave function becomes less than unity during the integration of the TDSE due to the absorbing boundary that is placed at the end of the radial grid. These absorbed parts of the wave function can be interpreted as representing true

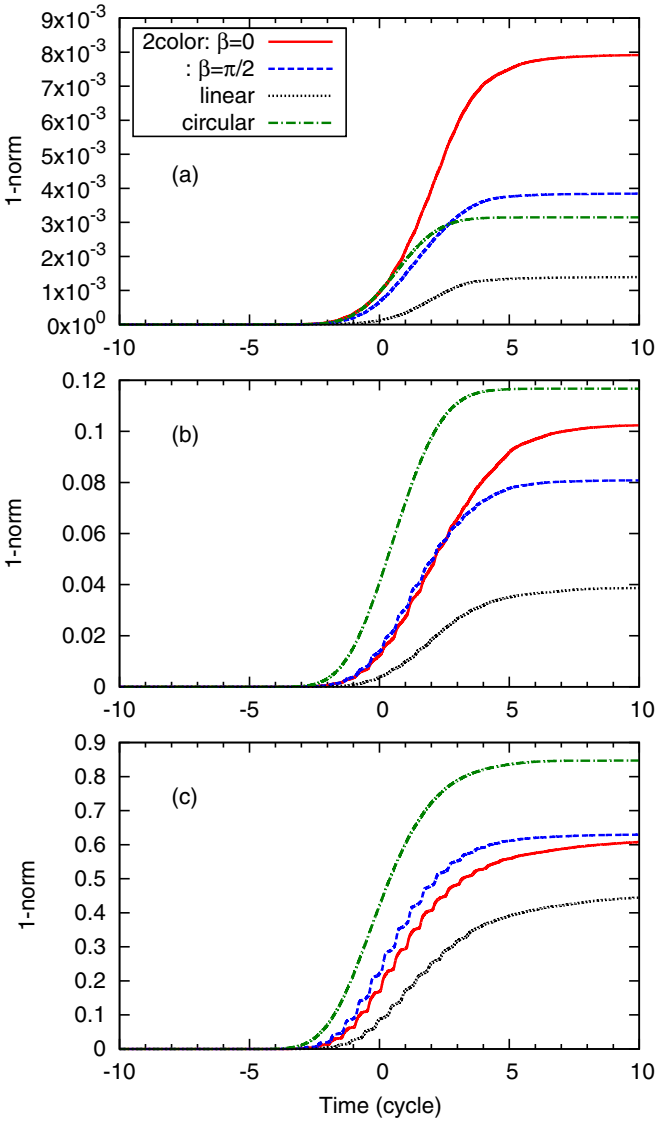

FIG. 1. (Color online) Change in the norm of the hydrogen-atom wave function driven by two-color (800 + 400 nm) orthogonal, linearly polarized (800 nm), and circularly polarized (800 nm) laser fields, respectively, for the peak fundamental-field intensities of (a) 5×10^{13} W cm^{-2}, (b) 1×10^{14} W cm^{-2}, and (c) 2×10^{14} W cm^{-2}. For all cases, the driving pulse contains 20 optical cycles (800 nm).

ionization, i.e., we can infer the total ionization probability from the change in the norm of the wave function. In Fig. 1, we plot the change in the norm during the time evolution when driven by two-color (800 + 400 nm) orthogonal fields defined by Eq. (7), for three different peak envelope intensities: $E_o^2 = 5\times10^{13}$, 1×10^{14}, and 2×10^{14} W cm^{-2}, and for two different phase delays: $\beta = 0$ and $\pi/2$, respectively. In addition, we compare with TDSE solutions for linearly and circularly polarized 800-nm laser fields, given by

$$\vec{E}(t) = E_o(t)[\hat{\mathbf{z}}\sin(\omega_o t) + \varepsilon\,\hat{\mathbf{x}}\cos(\omega_o t)], \qquad (28)$$

where $\varepsilon = 0$ and 1 for linear and circular polarization, respectively. We keep the same peak value E_o of the envelope function as for the two-color orthogonal fields.

The results in Figs. 1(b) and 1(c) are as expected, i.e., the atoms are ionized most by the circularly polarized fields and least by the linearly polarized fields, while the ionization rates for the two-color orthogonal fields lie in between. The lowest-intensity calculations in (a), however, predict more ionization in the two-color orthogonal fields than in the circularly polarized field. This implies that the 400-nm field, even though having only a quarter of the intensity of the 800-nm field, can become rather effective in ionizing electrons in the weak-field regime. This is understandable since a lower order in perturbation theory is required for ionization when the photon energy is doubled. In fact, harmonic spectra of helium atoms in Ref. [1] exhibit stronger even-order harmonics than odd-order ones in the plateau region, also indicating that the 400-nm field is quite capable of ionizing electrons when the binding force is comparably strong as the driving field, as in helium atoms. The phase delay β in the secondary fields seems to enhance the ionization in (a) and (b), but not for the highest-intensity calculations in (c). The difference due to the phase delay β is as large as $\sim$10% in (c) during the time evolution, indicating the importance of β in two-color orthogonal fields.

B. High-harmonic spectra

Figure 2 shows high-harmonic spectra generated by the 800 + 400 nm orthogonal fields of peak envelope intensity $E_o^2 = 1\times10^{14}$ W cm^{-2} for four different phase delays ($\beta = 0$, $\pi/4$, $\pi/2$, and $3\pi/4$). The vertical line indicates the position of the semiclassical cutoff in the linearly polarized 800-nm field of the same peak intensity, i.e., $I_p + 3.17U_p$, where I_p is the ionization potential of the atom, and $U_p = E_o{}^2/(4\omega_o{}^2)$ is the ponderomotive energy of the driving field [5]. The most striking feature in Fig. 2 is that the spectra evaluated from $\langle a_z\rangle$ and $\langle a_x\rangle$ exclusively appear at odd- and even-integer multiples of ω_o, respectively. This is due to the symmetry of interaction and holds true for any symmetry of the bound state [20]; cf. Eqs. (22) and (23). The intensities of the odd- and even-order harmonic spectra in 2(c) and 2(d) are equally strong in the plateau region, despite the fact that the peak driving-laser intensity in the x direction is four times smaller than in the z direction. This means that electrons contributing to these plateau harmonics are deflected by roughly 45° before returning to the atom, according to Eq. (24).

It is not obvious why even-order harmonics manage to have the same amount of intensities as odd-order ones in Fig. 2 and also in the experiments [1] and [3]. The ponderomotive energy U_p associated with the secondary field (along the x axis) alone would be only 1/16 of the fundamental field, but the x component of the acceleration vector can be equally large as the z component according to our calculation. In fact, the even-order harmonics measured in Ref. [1] were much stronger than the odd-order ones in the plateau region regardless of atomic species, helium or neon. In a semiclassical picture one can argue that a perhaps unexpected amount of direction change occurs along the electron trajectories. Additional studies based on the SFA [21], or the classical-trajectory analysis [22,23], are desirable in order to have a more intuitive understanding of the electron dynamics involved in the HHG driven by the two-color orthogonal fields.

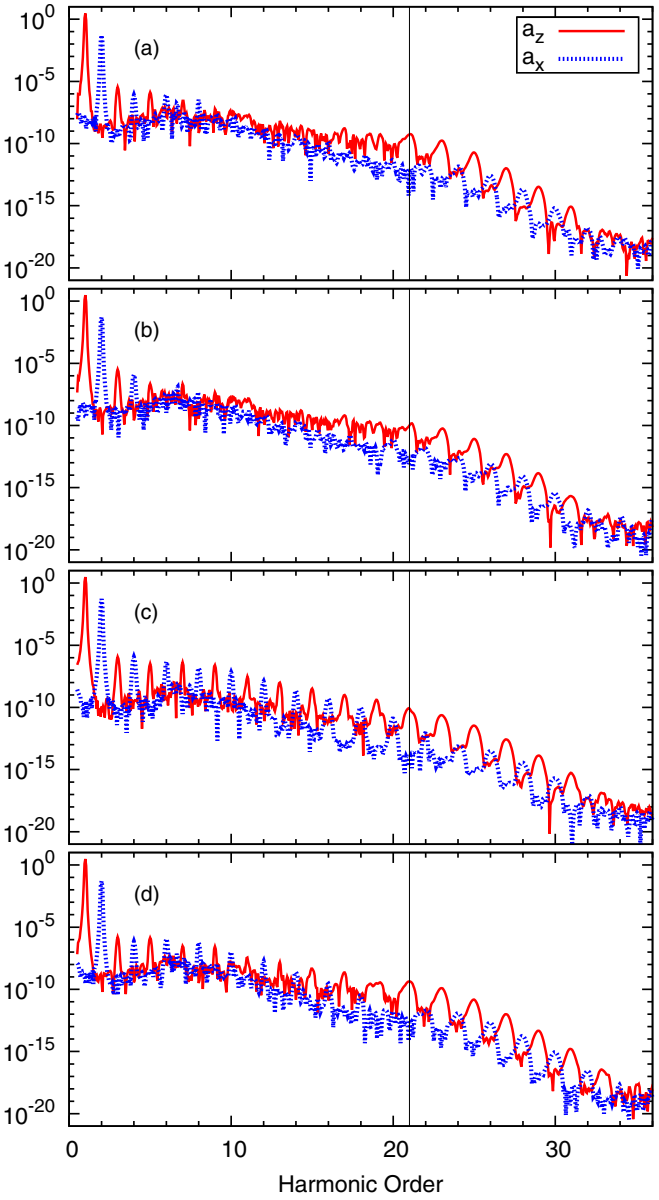

FIG. 2. (Color online) Hydrogen spectra driven by a 20-cycle, two-color (800 + 400 nm) orthogonal fields with (a) no phase delay ($\beta = 0$), (b) $\beta = \pi/4$, (c) $\beta = \pi/2$, and (d) $\beta = 3\pi/4$. The a_z and a_x contributions are shown separately; cf. Eq. (20). The peak intensity of the driving laser pulse is 1×10^{14} W cm^{-2} along the z axis and a quarter of that amount along the x axis. The vertical line indicates the location of the semiclassical cutoff for the linearly polarized 800-nm driving laser of peak intensity 1×10^{14} W cm^{-2}.

The spectral peaks in Figs. 2(a) and 2(b) are not as pronounced as in Figs. 2(c) and 2(d), indicating some interference from degenerate electron trajectories [24]. In Ref. [3], it was demonstrated in an experiment with argon atoms that the phase delay between the two orthogonal fields could be used to select the electron trajectory at the single-atom level, without the macroscopic propagation effect. In Sec. III D, we use the Gabor transform to elucidate this point.

A significant change in the overall shape of harmonics and in the position of the cutoff was observed in the experimental data of Ref. [1] for helium and neon atoms when the phase delay was varied between $\beta = 0$ and $\pi/2$. Our single-electron results in Fig. 2(b) do not suggest such an effect. This difference can be due to the macroscopic propagation and multielectron effects that are not included in our present calculation. We also note that the spatiotemporal profiles of the two orthogonal laser fields used in the experiment are not matching perfectly [20], i.e., may not correspond perfectly to the present calculation. We also note that the intensity ratio between the two fields was quoted as 3:1 in Ref. [20] rather than 4:1 [1].

C. Cycle-averaged recollision angles

Figure 3 displays collision angles as a function of phase delay between the two-color orthogonal fields, derived from the harmonic spectra (such as shown in Fig. 2) using Eq. (24). It represents the theoretical equivalent to the reported experimental recollision angles in Ref. [1] for helium and neon atoms. Note that the measurements only covered phase delays $0 < \beta < \pi/2$, whereas our phase delay extends up to π. One can also compare this plot with Fig. 3(b) in Ref. [10] or Fig. 1(b) in Ref. [11], where the intensity ratio of even/odd harmonic spectra for helium atoms is shown. There is clearly a common trend in these plots, namely, the region of large recollision angles protrudes to higher harmonic order between $\beta = \pi/4$ and $\pi/2$. When comparing with the path-integral calculation in Ref. [20], we find that our data in Fig. 3 capture some features of the experimental results for helium atoms in Ref. [1] more closely; e.g., the large ($\sim 80^\circ$) return angle for low-order harmonics is present in our calculations but not in the simulation of Ref. [20].

Our results for the hydrogen atom do not predict a dramatic change in the spectral intensities or in the cutoff frequency for various phase delays, in contrast to the finding of Ref. [1]. Whether our finding is specific to atomic hydrogen needs to be investigated. In the future, we intend to extend our calculation to multielectron atoms using time-dependent density-functional theory [25].

In addition, the effect of propagation needs to be addressed; in Ref. [1], the measured harmonic spectra contain purely

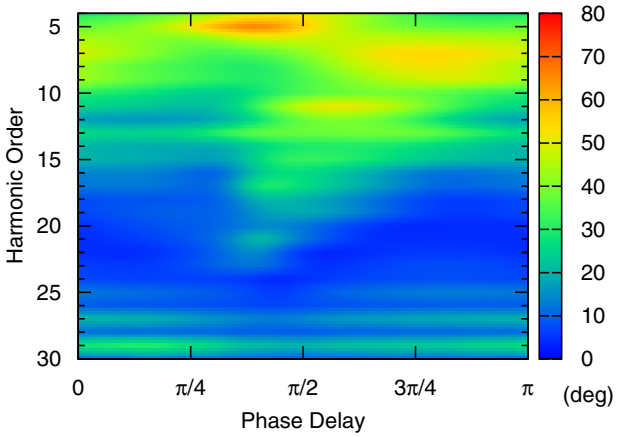

FIG. 3. (Color online) Recollision angles as a function of harmonic frequency (in units of the fundamental-field frequency ω_o) and phase delay between the two-color orthogonal fields, derived from hydrogen harmonic spectra using Eq. (24). The driving laser parameters are the same as in Fig. 2.

structural information not affected by electron-path interferences, because the short trajectories were macroscopically chosen by the focus of a gas jet. The single-atom calculation can achieve this goal by adjusting the relative phase β, but then β becomes no longer a variable to control electron dynamics. The complete understanding of experimental results requires a multielectron atom calculation coupled with Maxwell's equations to account for the variation of gas density along the laser beam [18].

D. Gabor analysis

In Ref. [3], it was found that the short-trajectory contributions dominate the high-harmonic spectra generated by two-color orthogonal fields when the nodes of the fundamental and secondary fields are set to coincide. In this section, we study the harmonic spectra in Figs. 2(a) and 2(c) by using the Gabor transform to shed some light on this question.

Figure 4 shows the return energy of a free electron driven by an 800-nm, linearly polarized field of peak intensity 1×10^{14} W cm^{-2} along the z axis, according to Newton's second law:

$$\ddot{z} = -E_o(t)\cos(\omega_o t). \tag{29}$$

The electron is released with zero initial velocity from the origin ($z = 0$) at various ionization times, and its return energy (shown in units of ω_o) is evaluated when it returns to the origin as the sum of kinetic energy and the ionization potential ($I_p = 13.6$ eV) that it had overcome. The results in Fig. 4 demonstrate that two degenerate trajectories occur periodically during each half cycle of the driving laser field; the ionization time in the rising (falling) side of the return energy corresponds to the long (short) trajectory in the SFA theory, whose recollision time is always in the falling (rising) side of the return energy

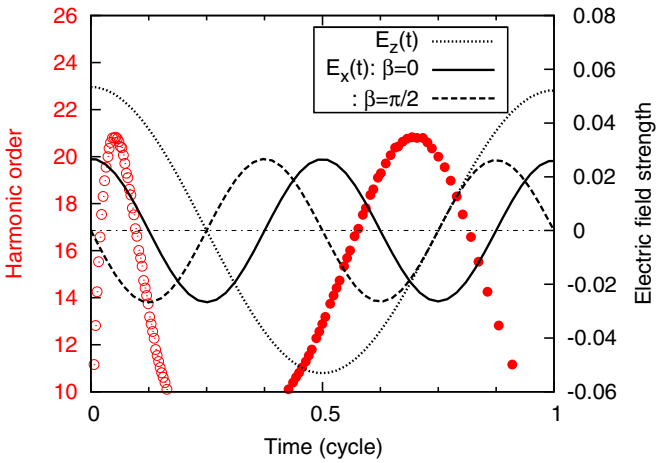

FIG. 4. (Color online) Open (closed) circles show the return energy of a free electron driven by an 800-nm linearly polarized field of peak intensity 1×10^{14} W cm^{-2} as a function of ionization (recollision) time, according to Eq. (29). For clarity, only those solutions that are released in the first half cycle after the pulse peak are shown. The energy is expressed in units of fundamental-field frequency ω_o. Also shown with different lines are the components of the two-color orthogonal fields (800 + 400 nm, $1/0.25 \times 10^{14}$ W cm^{-2}) with different phase delays: $\beta = 0$ and $\pi/2$.

in Fig. 4. The maximum return energy attained around the peak of a driving laser pulse ($\sim 21\omega_o$) is the semiclassical cutoff $I_p + 3.17U_p$ (cf. Fig. 2). Also shown in Fig. 4 is each of the two orthogonal fields for $\beta = 0$ and $\pi/2$. Note that the z component of the mutually orthogonal laser fields coincides with the linearly polarized field that was used to solve Eq. (29). In the supporting SFA theory of the experiment in Ref. [3] it was argued that the time when the electron is created in the continuum (i.e., ionization time) is relatively unchanged by the presence of the secondary field.

To find the recollision time of an electron according to the TDSE, we show in Fig. 5 the Gabor transform (25) of the high-harmonic spectra given in Figs. 2(a) and 2(c), corresponding to the phase delays of $\beta = 0$ and $\pi/2$, respectively. The timing of recollisions on the z axis inferred from the Gabor transform G_z (top panels) generally agrees with the classical recollision time in a linearly polarized field predicted by Eq. (29) (shown with closed circles in both Figs. 4 and 5), except that only the short trajectories appear when $\beta = \pi/2$. The differences between the quantum and the classical calculations are likely due to the initial conditions and the lack of binding potential assumed for the classical trajectories. The timing of recollisions on the x axis indicated by G_x (bottom panels) is periodic in each half cycle of the fundamental field when $\beta = \pi/2$, but not when $\beta = 0$; this behavior cannot be explained in terms of a one-dimensional approach such as Eq. (29).

The SFA calculation in Ref. [3] was based on the assumption that short trajectories give the main contribution to the harmonic spectrum when the ionization of the long trajectories happens before the peak of the secondary field; an ionized electron would then see the rising secondary field, making the recollision in the long trajectory less probable. This is when the nodes of the two orthogonal fields coincide, i.e., $\beta = \pi/2$ in our case. The agreement between our calculation and Ref. [3] is encouraging and lends support to the applicability of the SFA for two-color orthogonal fields.

E. Time-resolved recollision angles

From the Gabor transforms in Fig. 5, we calculated the time-resolved recollision angles of an ionized electron in two-color orthogonal fields by using Eq. (27). Figure 6 shows $|\theta_{\rm rec}(\omega,t)|$ (with respect to the fundamental-field direction) for $\beta = 0$ and $\pi/2$. Note that only those data points with $G_z > 10^{-15}$ are used to calculate Eq. (27). As a general trend for both cases, the recollision angles are larger in the plateau region than beyond the cutoff ($\sim 21\omega_o$), which is consistent with the cycle-averaged measurement using helium atoms in Ref. [1]. This agreement is expected because both the hydrogen and helium atoms are spherically symmetric.

Figure 6(a) for $\beta = 0$ shows irregular profiles in the plateau region, indicating multiple electron trajectories with large recollision angles. However, electrons contributing to the cutoff harmonics are all colliding with no deflection from the fundamental axis. On the other hand, Fig. 6(b) for $\beta = \pi/2$ exhibits fairly regular recollision angles occurring periodically in each half cycle of the fundamental field. The short trajectory is deflected by the secondary field by 30–45°, while the rest of trajectories are suppressed for the phase delay $\beta = \pi/2$; this coherent behavior was reflected in the clean spectra displayed

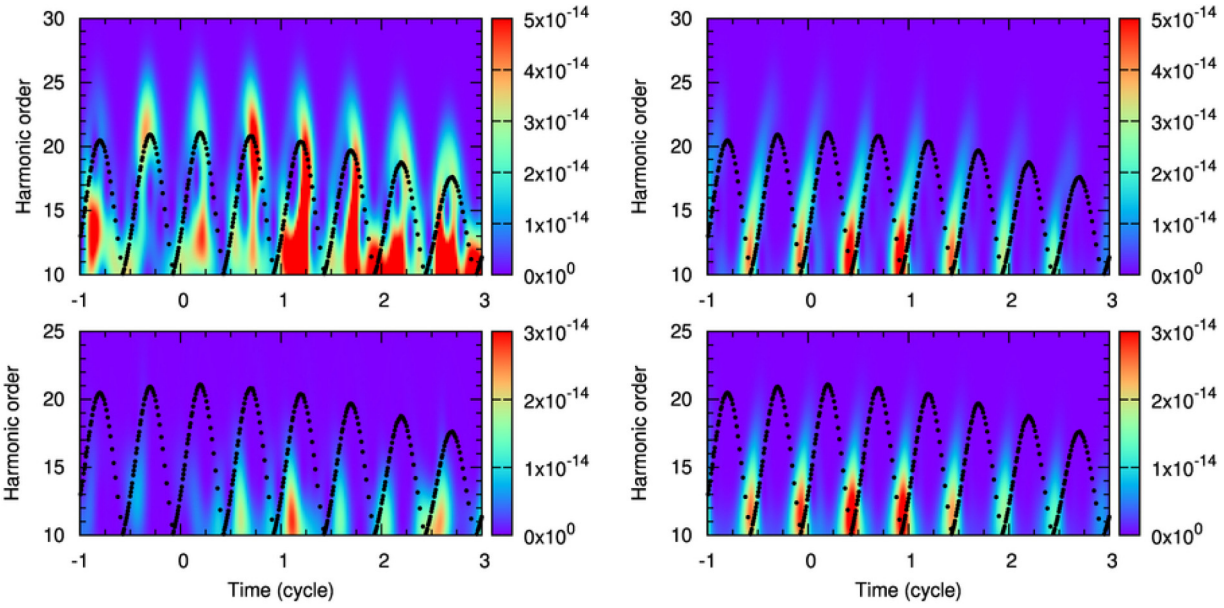

FIG. 5. (Color online) Gabor transform (25) of the harmonic spectra in Fig. 2(a) for $\beta = 0$ (left) and Fig. 2(c) for $\pi/2$ (right). The top panels are for the harmonic field polarized along the z axis, and the bottom panels are for the harmonic fields polarized along the x axis. The closed circles indicate the return energy of a free electron moving in a linearly polarized field along the z axis as a function of recollision time, according to Eq. (29).

in Fig. 2(c). It is also interesting that the return angles for cutoff harmonics are relatively large (10–20°) in Fig. 6(b) compared to Fig. 6(a). This means that, when there are no degenerate electron paths (as verified from clean harmonic spectra, e.g., beyond the cutoff in Fig. 2), the electron trajectories associated with each phase delay follow different directions that repeat in every half cycle of the fundamental field. The cycle-averaged measurements should therefore be able to deliver the structural information of target atoms by controlling the phase delays, as demonstrated in Ref. [1].

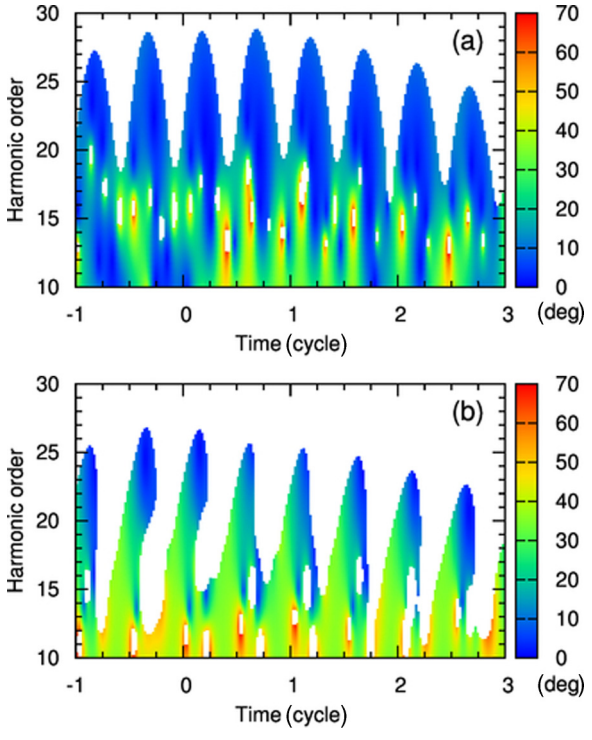

FIG. 6. (Color online) Recollision angle as a function of time and harmonic frequency (in units of ω_o), derived from the Gabor transforms in Fig. 5 using Eq. (27) for a phase delay of (a) $\beta = 0$ or (b) $\beta = \pi/2$.

IV. CONCLUSIONS

We studied HHG driven by strong two-color orthogonal fields based on the numerical solution of the 3D TDSE for the hydrogen atom. Our calculations lend support to the analysis of recollision angles reported in Ref. [1]. Furthermore, the time-frequency representation of the harmonic spectra was used to find the timing and direction of the recollision process in the chosen two-color orthogonal fields. We confirmed the finding in Ref. [3] that the short-trajectory contributions dominate the high-harmonic spectra at the single-atom level when the nodes of the fundamental and secondary fields are set to coincide. Our result is also in qualitative agreement with recent publications about the electron tunneling time for helium atoms [10,11].

ACKNOWLEDGMENTS

This work was partially supported by the U.S. Department of Energy. We also would like to acknowledge the partial support of the National Science Council of Taiwan and National Taiwan University (Grants No. 101R8700-2 and No. 101R104021). M.M. thanks Dr. S.-I Chu for the hospitality in his group, and S. Ohlmann for helpful discussions during the early stages of the work.

[1] D. Shafir, Y. Mairesse, D. M. Villeneuve, P. B. Corkum, and N. Dudovich, Nat. Phys. **5**, 412 (2009).
[2] H. Niikura, N. Dudovich, D. M. Villeneuve, and P. B. Corkum, Phys. Rev. Lett. **105**, 053003 (2010).
[3] L. Brugnera, D. J. Hoffmann, T. Siegel, F. Frank, A. Zaïr, J. W. G. Tisch, and J. P. Marangos, Phys. Rev. Lett. **107**, 153902 (2011).
[4] H. Niikura, H. J. Wörner, D. M. Villeneuve, and P. B. Corkum, Phys. Rev. Lett. **107**, 093004 (2011).
[5] P. B. Corkum, Phys. Rev. Lett. **71**, 1994 (1993).
[6] M. Abu-samha and L. B. Madsen, Phys. Rev. A **84**, 023411 (2011).
[7] M. Odenweller, N. Takemoto, A. Vredenborg, K. Cole, K. Pahl, J. Titze, L. P. H. Schmidt, T. Jahnke, R. Dörner, and A. Becker, Phys. Rev. Lett. **107**, 143004 (2011).
[8] J. Henkel, M. Lein, V. Engel, and I. Dreissigacker, Phys. Rev. A **85**, 021402(R) (2012).
[9] J. Itatani, J. Levesque, D. Zeidler, H. Niikura, H. Pépin, J. C. Kieffer, P. B. Corkum, and D. M. Villeneuve, Nature (London) **432**, 867 (2004).
[10] D. Shafir, H. Soifer, B. D. Bruner, M. Dagan, Y. Mairesse, S. Patchkovskii, M. Y. Ivanov, O. Smirnova, and N. Dudovich, Nature (London) **485**, 343 (2012).
[11] J. Zhao and M. Lein, Phys. Rev. Lett. **111**, 043901 (2013).
[12] X.-M. Tong and S.-I. Chu, Chem. Phys. **217**, 119 (1997).
[13] T. K. Kjeldsen, L. A. A. Nikolopoulos, and L. B. Madsen, Phys. Rev. A **75**, 063427 (2007).
[14] V. V. Strelkov, A. A. Gonoskov, I. A. Gonoskov, and M. Y. Ryabikin, Phys. Rev. Lett. **107**, 043902 (2011).
[15] X.-M. Tong and S.-I. Chu, Phys. Rev. A **58**, R2656 (1998).
[16] C. C. Chirila, I. Dreissigacker, E. V. van der Zwan, and M. Lein, Phys. Rev. A **81**, 033412 (2010).
[17] N. Schaeffer, Geochemistry, Geophysics, Geosystems **14**, 751 (2013).
[18] M. B. Gaarde, P. Antoine, A. L'Huillier, K. J. Schafer, and K. C. Kulander, Phys. Rev. A **57**, 4553 (1998).
[19] L. D. Landau and E. M. Lifshitz, *Quantum Mechanics*, Course of Theoretical Physics (Pergamon, Oxford, 1965), Vol. III Chap. 29.
[20] D. Shafir, Y. Mairesse, H. J. Wörner, K. Rupnik, D. M. Villeneuve, P. B. Corkum, and N. Dudovich, New J. Phys. **12**, 073032 (2010).
[21] M. Lewenstein, P. Balcou, M. Y. Ivanov, A. L'Huillier, and P. B. Corkum, Phys. Rev. A **49**, 2117 (1994).
[22] D. B. Milosevic, W. Becker, and R. Kopold, Phys. Rev. A **61**, 063403 (2000).
[23] P. J. Ho and J. H. Eberly, Phys. Rev. Lett. **95**, 193002 (2005).
[24] M. Lewenstein, P. Saliéres, and A. L'Huillier, Phys. Rev. A **52**, 4747 (1995).
[25] X.-M. Tong and S.-I. Chu, Phys. Rev. A **64**, 013417 (2001).